Science of the Total Environment 752 (2021) 141814

Contents lists available at ScienceDirect

Science of the Total Environment

journal homepage: www.elsevier.com/locate/scitotenv

A geostatistical fusion approach using UAV data for probabilistic estimation of *Xylella fastidiosa* subsp. *pauca* infection in olive trees

Annamaria Castrignanò [a], Antonella Belmonte [f,*], Ilaria Antelmi [i], Ruggiero Quarto [b], Francesco Quarto [c], Sameh Shaddad [d], Valentina Sion [i], Maria Rita Muolo [e], Nicola A. Ranieri [e], Giovanni Gadaleta [g], Edoardo Bartoccetti [h], Carmela Riefolo [a], Sergio Ruggieri [a], Franco Nigro [i]

[a] CREA-AA - Council for Agricultural Research and Economics (Bari, Italy), Via Celso Ulpiani, 5, 70125 Bari (BA), Italy
[b] Department of Earth and Geo-Environmental Sciences, University of Bari, Via Edoardo Orabona, 4, 70125 Bari (BA), Italy
[c] PRO-GEO s.a.s, Via M. R. Imbriani 13, 76121 Barletta (BT), Italy
[d] Soil science Department, Faculty of Agriculture, Zagazig University, 44511 Zagazig, Egypt
[e] Servizi di Informazione Territoriale S.r.l., Piazza Giovanni Paolo II, 8, 70015 Noci (BA), Italy
[f] CNR-IREA National Research Council - Institute for Electromagnetic Sensing of the Environment (Bari, Italy), Via Amendola, 122/D, 70126 Bari, Italy
[g] Professional Agronomist, Via Carr. Lamaveta, 63/F, 76011 Bisceglie (BT), Italy
[h] Salt & Lemon, Piazza Mascagni 11, 10015 Ivrea (TO), Italy
[i] Department of Soil, Plant and Food Sciences, University of Bari - Aldo Moro, Via G. Amendola 165/A, 70126 Bari, Italy

HIGHLIGHTS

- The site-specific management of Xylella infection involves the use of different monitoring tools.
- A data fusion approach was defined which effectively combines heterogeneous multi-source data.
- The approach is based on non-parametric multivariate geostatistics and provides a probabilistic map of infection risk.
- Joint analysis of data with different spatial resolution involves the problem of "change of support".
- The phenomenon of Xylella infection is essentially punctual and all measurements should be carried out at a very fine scale.

GRAPHICAL ABSTRACT

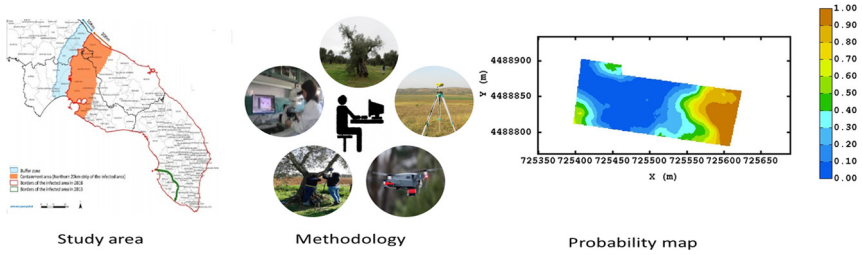

ARTICLE INFO

Article history:
Received 8 June 2020
Received in revised form 17 August 2020
Accepted 18 August 2020
Available online 23 August 2020

Editor: Elena Paoletti

Keywords:
GPR
Trunk survey

ABSTRACT

Xylella fastidiosa is one of the most destructive plant pathogenic bacteria worldwide, affecting more than 500 plant species. In Apulia region (southeastern Italy), *X. fastidiosa* subsp. *pauca* (*Xfp*) is responsible for a severe disease, the olive quick decline syndrome (OQDS), spreading epidemically and with dramatic impact on the agriculture, the landscape, the tourism, and the cultural heritage of this region. An early detection of the infected plants would hinder the rapid spread of the disease. The main objective of this paper was to define a geostatistical approach of data fusion, which combines remote (radiometric), and proximal (geophysical) sensor data and visual inspections with plant diagnostic tests, to provide probabilistic maps of *Xfp* infection risk. The study site was an olive grove located at Oria (province of Brindisi, Italy), where at the time of monitoring (September 2017) only few plants showed initial symptoms of the disease. The measurements included: 1) acquisitions of reflected

* Corresponding author at: CNR-IREA Via Amendola, 122/D, 70126 Bari, Italy.
E-mail address: belmonte.a@irea.cnr.it (A. Belmonte).

https://doi.org/10.1016/j.scitotenv.2020.141814

PCR
Polygon cokriging
Probability kriging
Radiometric data

electromagnetic radiation with UAV (Unmanned Aerial Vehicle) equipped with a multi-spectral camera; 2) geophysical surveys on the trunks of 49 plants with Ground Penetrating Radar (GPR); 3) disease severity rating, by visual inspection of the proportion of canopy with symptoms; 4) qPCR (real time-quantitative Polymerase Chain Reaction) data from tests on 61 plants. The data were submitted to a set of processing techniques to define a "data fusion" procedure, based on non-parametric multivariate geostatistics. The approach allowed marking those areas where the risk of infection was higher, and identifying the possible infection entry routes into the field. The probability map of infection risk could be used as an effective tool for a preventive action and for a better organization of the monitoring plans.

1. Introduction

The olive quick decline syndrome (OQDS) is a devastating vascular disease caused by *Xylella fastidiosa* subsp. *pauca* (*Xfp*), a rod-shaped, Gram-negative, and quarantine bacteria for the European Union. The bacterium is naturally transmitted by insect vectors of the family *Aphrophoridae*, which feed on the xylem of host plants. As a xylem-limited bacterium, *Xfp* clogs the vessels, thus causing rapid dieback of shoots, twigs and branches, and leading to death of the tree. Leaf tips and margins turn dark yellow to brown, tissue discoloration then spreads inward, leading to necrosis of the blade. Symptoms usually progress in severity from the older to the younger leaves on a branch; leaf symptoms may be localized to a single limb or sector of the tree, or may extend to the whole canopy. Xylematic vessels of the affected organs (twigs, branches, and trunks) show discolorations. Dark streaks and brown stains occur in the sapwood and in the vascular cambium. The disease appeared few years ago, in a grove located near the city of Gallipoli, on the Ionian coast of the Salento peninsula (Apulia region, south-east Italy), and spread fast towards the North, in the provinces of Brindisi and Taranto (Saponari et al., 2013). To date, *Xfp* spread on more than 40% of the Apulian territory, covering an area with more than 20 million of olive trees (Saponari et al., 2019). This has resulted in very serious losses to oliviculture, one of the main productive sectors of Apulia, with a remarkable impact on environment, landscape protection, and cultural heritage of that territory. Subsequently, the disease has also been reported in France (Menton), and in Spain (Balearic Islands and community of Madrid), the latter being the world's leading olive producer country, with approximately 2.7 million hectares of olive trees, 55% of its cultivated area (European Parliament, November 2019). Considering the global olive cultivated area in the EU, projections of future economic impact in affected countries reach billions of Euros (Schneider et al., 2020). Being a quarantine pathogen for the EU territory, control measures are under the coordination and responsibility of the Phytosanitary Authorities, and to date they rely on containment and mitigation measures, such as monitoring, sampling, diagnostic tests, removal of infected trees, and vector control interventions (Saponari et al., 2019; www.emergenzaxylella.it). Moreover, there is not yet unequivocally accepted cure against this lethal bacterium, and a serious risk exists that the bacterium spread throughout the whole Europe, particularly the countries of the Mediterranean Basin (Schneider et al., 2020). Furthermore, climate change seems to trigger environmental conditions that are particularly favorable to the spread of the bacterium in the most important olive growing areas of the Mediterranean Basin (Bosso et al., 2016). Best practices to control the disease should then focus on early detection of infection, preferably before the symptoms of the disease are visible, so that decisions on preventive actions can be made in a timely manner. However, for the effectiveness of such actions it is necessary that the diagnosis is based on an investigation at a very fine spatial scale, even within a single plant, and covers large extensions. Field surveys have already been extensively used in the past for pest detection but they are destructive, labor-intensive, time consuming, and unsuitable for large-scale spatial and temporal monitoring. Furthermore, as stated in a recent document prepared by European Food Safety Authority (EFSA) at the request of the European Commission, about specific guidelines for the survey of Xylella fastidiosa (TECHNICAL REPORT, APPROVED: 27 May 2020, doi:https://doi.org/10.2903/sp.efsa.2020.EN-1873), Xylella fastidiosa is known to exhibit a long asymptomatic period (in olive trees even longer than one year).

Therefore, if surveys rely on visual inspection only, *X. fastidiosa*-infected trees might escape when the plants are asymptomatic, or might be detected at an advanced stage of the disease, when the plants already served as source of the inoculum for the infection of the adjacent trees.

Remote Sensing was used extensively to detect and evaluate the disease severity for different crops and comprehensive reviews are available (e.g., Barton, 2012; Jackson et al., 1993; Sankaran et al., 2010; West et al., 2003; Zhang et al., 2019; Calderón et al., 2013; Mahlein et al., 2012; Gold et al., 2020).

Satellite remote sensing was also widely used for the detection of plant water stress (Kogan, 1995; Seguin et al., 1991), which is a phenomenon strongly related to OQDS, by utilizing visible and near infrared (VNIR) (Ghulam et al., 2008), thermal infrared (Anderson et al., 2012; Han et al., 2016; Sagan et al., 2019), and microwave bands (Chakraborty et al., 2016; Steele-Dunne et al., 2017). However, current satellite platforms have various limitations if their data are applied for early detection of plant disease, or more generally, for crop physiology monitoring, mainly due to too coarse spatial resolution and/or insufficient revisit frequency (Sagan et al., 2019). An effective campaign to contain the epidemic spread of the bacterium, may require monitoring even on a daily basis regardless of weather conditions, such as cloudiness and rain, which can affect the quality of the radiometric signal. Moreover, in order to reduce the presence of mixed pixels, that blend soil, plant and possible other objects, it is necessary to operate with moderate resolution satellites, such as Lansat-8 and Sentinel-2. They might have a sufficient spatial resolution, but have a revisit time of 5–16 days, too long for the early detection of plant disease stress not yet visible with naked eye (asymptomatic plants). Lack of early detection may cause the disease to evolve in stages where it is impossible to recover the plant, or at least to contain the spread of the pathogen, thus causing large-scale epidemic disease.

UAV may be a beneficial solution if very fine scale plant monitoring is to be used to detect disease in asymptomatic plants or at a very early stage of infection (Maimaitijiang et al., 2020). Over the last few years UAVs or drones have become one of the world's most talked about technologies. The UAV technology is born not to replace the manned aircraft or satellites acquisitions but to give support with its large of advantages to the more traditional remote-sensing methods.

UAV can collect images under cloud cover at very high resolution and with much more detail than satellite images. UAV is easy to use and can operate almost autonomously. In addition, there is currently a growing number of fairly friendly and inexpensive programs of data processing. The versatility of drones provides many different avenues for improving upon existing agricultural processes, including i) soil and field analysis (e.g., Paredes et al., 2017; Allred et al., 2018), ii) crop monitoring (e.g., Zheng et al., 2016), iii) irrigation (e.g., Santesteban et al., 2017), iv) crop spraying (e.g., Faical et al., 2014; Dai et al., 2018),

v) aerial seeding (e.g., Buters et al., 2019; Andrio, 2019), and last but not least, vi) health assessment (e.g. Kerkech et al., 2018).

However, the use of one sensor or type of vegetation measurement might be of limited value to obtain information on the health status of a plant, due to the multiple processes and complex interactions that take place at the onset of the bacterium infection. Various sensor methods have been used and assessed individually as alternative diagnostic tools (Berdugo et al., 2014), but the future challenge is to combine multi-source information into a more effective indicator of Xylella occurrence.

Recently GPR was used for detection and measurement of internal defects and reconstruction of the internal structure for tree trunks, especially of old and rare trees (Fu et al., 2014; Wen et al., 2016; Li et al., 2018; Barone and Ferrara, 2019). GPR uses the principle of scattering of electromagnetic wave, which propagates through the medium and is reflected from an object. The velocity of the scattered signal is mostly determined by the permittivity of the material, which is influenced by water content and density. Therefore, the sensor response, convoluted over space – time at plant scale, could be used as an indicator of the aridity conditions of the trunks.

Multiple sensing data could be then advantageously used as auxiliary information, to supplement sparsely sampled data of a laboratory variable for assessing bacterium infection risk, with a view to planning some preventive action of plant recovery. This process of fusing heterogeneous spatial data can be done statistically by defining a specific indicator of plant infection, and developing a methodology for appropriately weighting and combining it with a set of auxiliary information, assumed as relevant to the process of interest, in order to improve the accuracy of risk prediction (Zovko et al., 2018; Shaddad et al., 2020). Risk assessment consists in observing the occurrence of infection, and predicting it at un-sampled locations with an estimated level of uncertainity. A probabilistic approach is preferred because risk assessment is generally based on the estimation of variables, which are subject to great uncertainty (Castrignanò et al., 2008), due to the extremely random nature of the disease spread and the unavoidable limitation of sampling.

Non-parametric geostatistics is a set of statistical techniques that put as priority the modelling of uncertainty (Journel, 2011; Goovaerts, 1997). More specifically, modelling the probability of occurrence at any unsampled location is related to the proportion and location of the neighbouring data where the same phenomenon occurs. A non-parametric approach, called probability kriging, was proposed by Journel (2011), which is based on cokriging estimator and uses all available information from all different attributes to improve the prediction of probability of occurrence. Geostatistics allows also to solve the crucial problem called “the change of support”, that arises when two or more variables with different support have to be integrated in a way that permits valid inferences. The term “support” in geostatistics is associated to size, shape and spatial orientation of the unit region which the measure applies to (Guthrie and Olea, 1991). Many of the statistical solutions to this problem were developed by Matheron (1963) in block (co)kriging, which probability kriging is related to, but there is presently a lack of effective applications in the field of plant infection.

In the light of the above considerations, the main objective of this paper was to describe and apply a novel risk assessment method, based on multivariate non-parametric geostatistics, which combines remote (radiometric) and proximal (geophysical) sensor data with visual inspection data and plant diagnostic tests, to provide probabilistic maps of *Xfp* infection in olive trees, that can actually support containment of this pathogen.

2. Materials and methods

2.1. Study site

In order to deal with the spread of OQDS in southern Apulia, and based on the Commission Implementing Decision (EU) 2015/789, the regional Phytosanitary Authority delimited three different areas: 1) the infected zone, including the area where the disease had been diagnosed initially; 2) the containment zone, including the last 20 Km towards North of the infected zone, where in some cases, the eradication of olive trees is established; 3) the buffer zone, i.e. the outermost area (about 30 Km from the infected zone), which is not yet contaminated, and where the aim is to avoid contamination.

The study site was a commercial, centenarian, olive grove (cv. Ogliarola Salentina) located at Oria (province of Brindisi, south-eastern Italy), and placed between the infected and the containment zones at the time of monitoring (September 2017). The experimental field was chosen because the monitoring of both healthy and infected plants over time was possible without the infected plants were cut down. At the beginning of data collection, only few centenarian olive plants showed initial symptoms of the disease (wilted shoots).

2.2. Monitoring network and data

The measurements included:

1) Acquisition of reflected electromagnetic radiation with UAV.

The aerial surveys were conducted using a DJI Mavic Pro drone: a very light quadcopter equipped with on-board Global Navigation Satellite System (GNSS) and able to perform programmed missions over waypoints routes. A custom payload tray was designed to carry the multispectral sensor (Parrot Sequoia) on the bottom part of the UAV, and Sequoia's Sunshine Sensor, that integrates also an Inertial Measurement Unit (IMU) a Magnetometer and a Global Positioning System (GPS), on the top part. Parrot Sequoia camera captures high resolution RGB images (16 Megapixel) and four narrowband spectral images in green (550 ± 20 nm), red (660 ± 20 nm), red-edge (735 ± 5 nm) and near infrared (790 ± 20 nm) spectral bands at a resolution of 1.2 Megapixel. This type of sensor, although limited in the number of bands and spectral resolution, represents a good cost-effective solution and is also widely used in precision agriculture applications.

The data collection flight was planned on September 20, 2017, at 70 m height, with a theoretical resulting Ground Sampling Distance (GSD) of 6.6 cm/pixel.

Flight mission was programmed using Mission Planner software: a simple grid pattern with both 80% frontal and lateral overlap was designed to optimize photogrammetric data collection. The mission was then uploaded to Litchi ground-station controller software on an Android smartphone connected to UAV remote controller.

In order to increase absolute geospatial accuracy of maps generated with Structure-from-Motion (SfM) software, a ground survey was conducted over 10 ground control points in cross-format of approximately 50 cm $\times$ 50 cm size, distributed equally in the experimental area. The coordinates of these targets were measured with a Leica GPS1200, dual-frequency in real-time kinematic (RTK) mode, with sub centimeter precision.

The dataset consisted in 288 aerial shoots for each multispectral band, for a total of 1152 images and two additional shots (before and after every flight) at the radiometric calibration target that was provided with Sequoia camera.

Images elaboration was performed using Pix4d Mapper Pro software, that uses SfM techniques for the reconstruction of the scene (Nex and Remondino, 2014) on the basis of a large number of overlapped photos.

2) Geophysical surveys.

The surveys were carried out with a GPR on the trunks of 49 plants among the 61 trees of the groove. Those excluded showed trunks so irregular and cracked that it was impossible to investigate. The device was positioned in contact with the bark of the trunk, and moved along a longitudinal path from top (branch) to bottom (tree base), which was chosen because it was the flattest, uniform and free of apparent discontinuities (bulges or voids along the trunks).

Given the very irregular shape of the trunks of centenarian olive trees, it was not possible to adopt a single criterion for investigating the plants. This means that it was possible to use neither the same height above ground for the starting point, nor the same height above ground for the stopping point nor the same orientation for all the radar profiles. Very simply the best route was chosen, which was sometimes the only one possible. The surveys were carried out using the Noggin 500 radar (Sensor&Software Inc.), with the technical characteristics reported in Table S1 (supplementary material).

To obtain good quality in the recordings, the parameters associated with duration, depth of investigation, wave speed and impulse energy were set in advance (Table S1, supplementary material).

Pre-processing of data was performed using the following procedures:

- SETTING TIME ZERO: since the acquisition starts before the radar pulse is emitted, the zero of time must be set. This is identified on the basis of the arrival of the air radar wave moving from the transmitting antenna to the receiver: 0.5 ns before the arrival, because the distance between the antennas was 0.15 m.
- DEWOWING: Wow is a very low frequency noise present in radar recordings. It occurs because of saturation of the recording instrument's electronics with the large amplitudes of the air and direct radar waves. Residual Mean Filter implemented the wow removal, where the mean value of the surrounding filter point samples was subtracted. It works as High Pass Filter. A previous spectral analysis was performed to choose the frequencies to be removed below the specified High Pass Frequency.
- FILTERING: Frequency filtering was performed with Gaussian method, using the central frequency of the device (500 MHz), a width of 1.5 octaves (0.75 octaves on both sides of the spectrum), and 70 points in the time-domain operator, with constant phase spectrum and a parzen smoothing (Sheriff, 2002; Parzen, 1962; Percival and Walden, 1993).
- FK FILTERING: A two-dimensional FK filters both temporal and spatial frequencies and is typically used to remove coherent noise. A FK velocity filter (pie-slice filter) was used, both in positive and negative K-space, for removing both the air waves reflections (about 0.30 m/ns), due to the trunks and branches of the olive trees, and reflections due to localized defects in the trunks, with velocity lower than 0.12 m/ns.

The above four procedures were performed with GRADIX software (Interpex Ltd.).

- ENVELOPE: it was used to calculate the instantaneous amplitude of the radar signal and was performed with Hilbert Transform method, which enhances the reflection strength of the radar energy; it was performed with EKKO 42 software (Sensors & Software).

3) A visual rating of the canopy showing disease symptoms (leaf scorching, chlorotic discoloration of the canopy portion) was also carried performed at the same date of the UAV flight.

The proportion of symptomatic canopy was estimated at each of the four cardinal sites sides of the tree.

4) PCR molecular tests (binary data: healthy, infected) were done on 61 plants at the same date of the UAV flight to detect the presence of infection. The detection of the presence of *X.f.*, was carried out using the molecular methods allowed by the current phytosanitary regulations (PCR-end point for a qualitative result (healthy/infected) and real-time PCR (qPCR) for a quantitative measure of the bacterial DNA in the tissues examined (Rodrigues et al., 2003; Francis et al., 2006). The continuous measurements of qPCR (quantitative Polymerase Chain Reaction) were repeated in March 2018 to evaluate the progress of infection.

Portion (1 g) of hardwood cuttings were surface disinfected and used to extract Total Nucleic Acid (TNA) following a standard CTAB-based procedure (Loconsole et al., 2014). Aliquots of 2.0 μL of TNA were tested in triplicate by quantitative real-time PCR (qPCR) in 25.0 μL of final reaction volume, according to the protocol of Harper et al. (2010), and using a CFX96 Touch Real-Time PCR apparatus (Biorad, Hercules, CA, USA). As positive controls, DNA from a pure culture of *X. fastidiosa* subsp. *pauca* ST53 growing on buffered charcoal yeast-extract agarized medium (BCYE) was used (Saponari et al., 2017). Data about *Xfp* level occurring in the tested plants was expressed as concentration of the bacterial DNA (ng μl^{-1}) determined by interpolating the mean value of the cycle threshold (Ct) with the standard curve from a serial dilution (10–10^{-7} ng μl^{-1}) of pure bacterial DNA. Ct values ≥38 were considered negative.

2.3. Data analysis

The processing of the multi-source data included different steps.

2.3.1. Automatic extraction of canopy polygons from UAV data

The flowchart of methodology is showed into Fig. 1.

The processing and the subsequent analyses of images to extract the information about the delimitation of olive trees crowns have been carried out using the ENVI 5.1 software. The open source software QGIS has been used to define each polygon structure of vector data.

1) Layer stacking

The images have been first stacked; in this way all UAV bands have been merged into a single multispectral image. In order to do that it is required that the images have to have the same extent (number of rows and number of columns). In other words, it is needed that all images/bands have the same spatial resolution to be able to perform layer stacking.

2) Colours composition

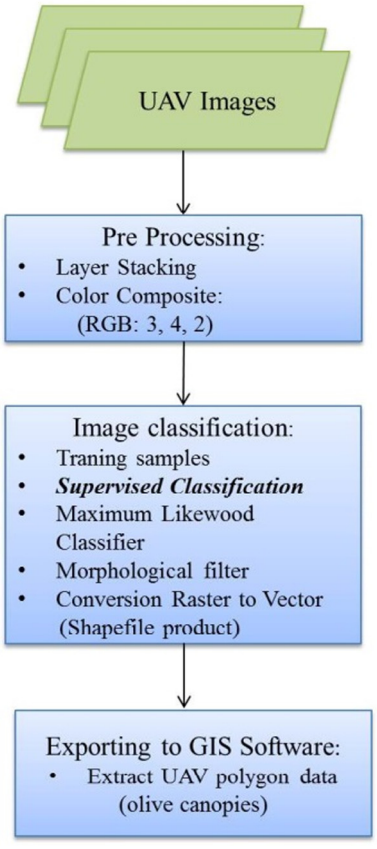

Fig. 1. Flow chart of semi-automatic extraction UAV polygon data.

The stack of different bands of the electromagnetic spectrum have been displayed on the computer screen as coloured pictures. For multispectral images any spectral band was associated with the visualization colours to favour a more accurate photointerpretation process, that is the best extraction of specific information about objects properties, such as stress and vigour of vegetation. In this regard, to emphasize the state of the plant (specifically the foliage of the olive trees) the following false colour composition has been applied: Red → Red, Red Edge → Green, Green → Blue.

3) Supervised classification

The processing core was the supervised classification. The following procedure has been used to select thematic information:

– Training samples

To select thematic information, the set of ground cover types (information class) into which the image had to be segmented, was firstly decided. Then, the prototype pixels (training samples) were assigned to the selected classes. For this study three classes, that were taken from different but sufficiently homogeneous areas of the same image, were identified as training classes: soil, canopy and shadow. In order to take the variability of the classes into account and avoid transition areas between the classes with mixed pixels (Campbell and Wynne, 2011), it was necessary to select a sufficient number of training pixels (minimum 150 pixels per class). In this way, a properly representative sample of each class was obtained.

– Maximum likelihood

The training data were used to estimate the parameters of the particular classifier algorithm. The maximum likelihood with Gaussian model has been applied as decision rule. As result a thematic map, in which the required classes appeared, has been produced.

– Morphological filter

To preserve the geometric structure of the image objects, a morphological filter, based on closing operator (Nixon and Aguado, 2012), was applied. This operator type has the function of modifying the geometry features of the signal, removing small holes inside the polygon. A morphological convolution is applied to the signal with a structuring element, which is another set of simpler shape and size (Diggle and Serra, 1983; Lantuéjoul and Serra, 1982; Sternberg, 1983; Maragos, 2009).

– Conversion raster to vector

The smoothed data were converted from a labelled raster image into vector data format (such as ESRI Shapefile format). This step was indispensable for later spatial analysis.

4) Exporting to GIS software

Each closed polygon representing one plant was imported into GIS environment and an editing procedure was applied to generate a multipolygon product. These processes allowed to modify the vertices of the selected geometry, to fill eventual holes in the polygon and to cut part of the geometry. The extracted 61 polygons (Fig. S1 supplementary material) were marked with numbers representing each olive tree, which were used for all (radiometric, geophysical, visual and laboratory) types of measurements. In order to georeference the trees, the gravity centre coordinates were assigned to them.

2.3.2. Geostatistical interpolation of trunk radar data

The 2D spatial-temporal trunk data acquired with GPR, after pre-processing, were submitted to geostatistical procedures to provide a spatial temporal map of the radar signal (IP). As the GPR data showed sensible departure from normal distribution, they were previously transformed into Gaussian equivalents through Gaussian anamorphosis, using a truncated series of Hermite polynomials (Castrignanò et al., 2017). After that a directional experimental variogram was calculated along the horizontal-temporal direction and the vertical-spatial direction (oriented from the ground upwards), to which a theoretical mathematical model was fitted. Finally ordinary kriging was applied for interpolations and the estimates were then back-transformed to the raw data of each plant for display.

2.3.3. Change of support

The collected multi-source data had different supports: i) UAV pixel size of 0.07 m × 0.07 m; ii) trunk radar data: approximately 0.01 m × 1 ns; iii) visual inspection and laboratory data as point data at plant level, before jointly analyzing them, it was necessary to refer them to the same support using polygon kriging (Diacono et al., 2014; Landrum et al., 2016). Polygon (co)kriging procedure was used to provide the expected value and standard deviation of the study variables for each plant (polygon) of the olive grove. Polygon (co)kriging technique is an extension of block (co)kriging (Goovaerts, 1997) using a special neighborhood. It estimates the expected value of a variable over an irregular shape (i.e., the polygon of each plant canopy) and its standard deviation. The polygon is first discretized in regular cells υ_i, after that the procedure is quite similar to that of block kriging, except for the calculation of the average co-variance function ($K_{\alpha v}$) for each polygon v, which is calculated as a weighted discrete summation:

$$K_{\alpha v} = \frac{1}{\sum_i \omega_i} \sum_{i=1}^{N} \omega_i K_{\alpha c_i} \tag{1}$$

where each weight ω_i corresponds to the surface of intersection between the cell v_i centered in the point c_i and the polygon v, α is a data point, and $K_{\alpha ci}$ is the covariance function calculated at each point c_i.

Therefore UAV and radar data had to be previously transformed to aerial data at plant level using polygon kriging (Fig. 2). For UAV data, the polygons were those previously extracted for each plant from the raster images; whereas a single rectangular polygon with dimensions 7 ns × 1.50 m was used for the radar data. The size was determined by the time of signal propagation across the trunk before it was significantly attenuated by multiple backscattering, and by the average length of the surveyed trunk profile.

2.3.4. Geostatistical multi-source data fusion for probabilistic mapping of infection risk

Once all the eleven: laboratory (Indicator), visual (N, E, S, W sectors), radiometric (Green, Red, Rededge, NIR bands), geophysical (IP and its standard deviation, std_IP) variables were reduced to the same support (plant), they were jointly submitted to the multivariate geostatistical approach of data fusion.

The proposed geostatistical method is based on a simple binary transformation, whereby each datum of the PCR measurement, assumed as criteria to evaluate infection risk, is transformed into an indicator, i.e. a binary value coded as 0 for healthy plant or 1 for infected plant (Shaddad et al., 2020).

The unknown value of indicator in an unsampled point can be estimated as a weighted average of the neighbouring indicator data using indicator kriging (IK) (Goovaerts, 1997). However, IK uses only the information extracted from PCR analyses rather than all the information gathered relating to the process of bacterium infection. Probability Kriging (PK) (Journel, 2011) is an enhancement of indicator kriging, because it uses both secondary information (visual, UAV, radar data) and the primary variable (indicator information from PCR measurements) at each sampled plant location x_α in a multivariate approach, called co-indicator kriging. In our case, the target variable is a binary variable with values of either 0 or 1, whereas the covariates (multi-type monitoring data) are continuous numerical variables. Due to the large differences between the units of measurement of secondary variables and those of indicator variables, cokriging system may suffer from instability

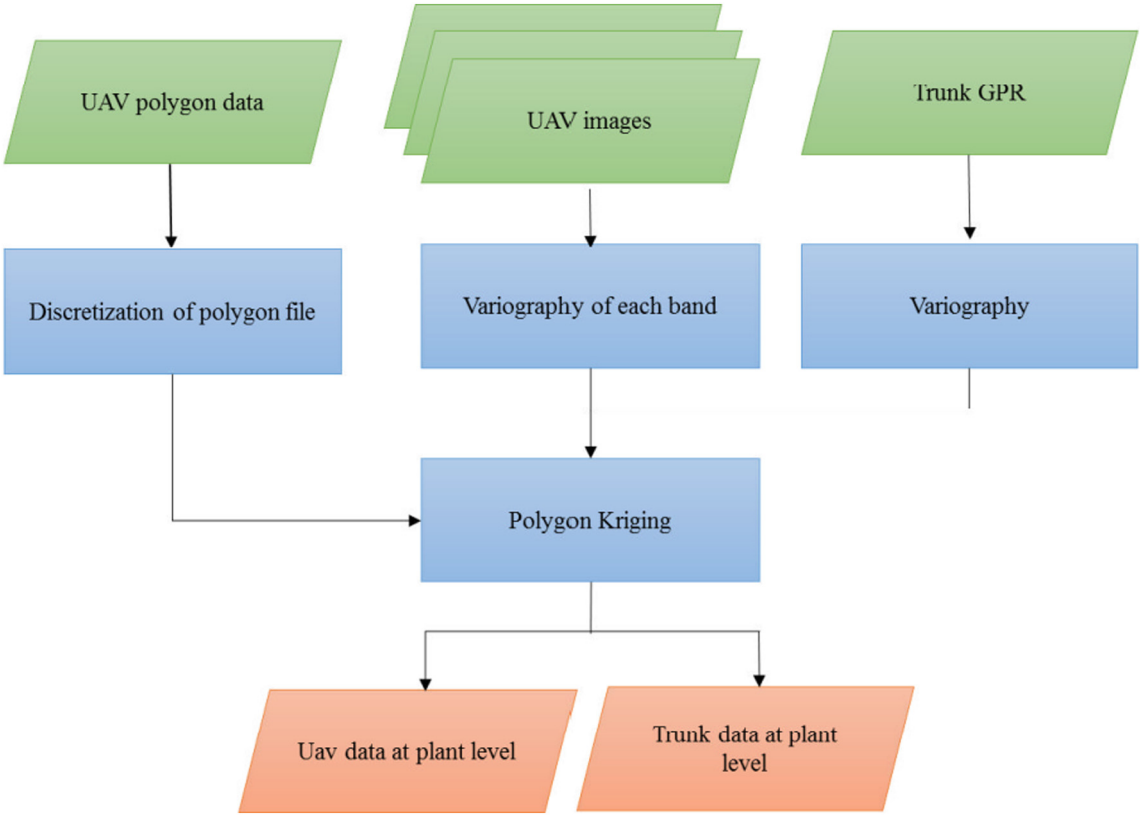

Fig. 2. Flow chart of polygon kriging outputs.

problems during resolution. Therefore, further data transforming is required.

Since indicator data $i(x_\alpha)$ are valued either 0 or 1, it is necessary to first transform the auxiliary variables $z(x_\alpha)$ to the range [0 to 1] through relative rank order transform (Journel, 2011):

$$k(x_\alpha) = \frac{r(x_\alpha)}{N} \tag{2}$$

where $r(x_\alpha)\epsilon(1,N)$ is the rank of the datum $z(x_\alpha)$, when data are ranked in increasing order, and N the total number of sample locations.

To apply PK approach, it is required fitting a linear model of coregionalization (LMC) (Wackernagel, 1995; Castrignanò et al., 2017) to the whole set of experimental semivariograms including both direct semivariograms of indicator and rank-order transformed variables, and cross-semivariograms between each pair of variables, regardless of its type (indicator or rank) (Shaddad et al., 2020).

PK is then the ordinary co-kriging of the indicator transform $i(x_\alpha)$ and the rank-order transform $k(x_\alpha)$ of each secondary variable. The probability kriging estimate $i^*(x_0)$ at each unsampled point x_0 is given by:

$$i^*(x_0) = \sum_{\alpha=1}^{n_1} \lambda_\alpha(x_0) i(x_0) + \sum_{j=1}^{n_b} \sum_{\alpha=1}^{n_j} \nu_{\alpha,j}(x_0) k_j(x_\alpha) \tag{3}$$

where n_1 and n_j are the number of observations of indicator and rank-order transformed variable j within the neighborhood of x_0, respectively; n_b is the number of secondary variables to take into account. The weights $\lambda_\alpha(x_0)$ and $\nu_{\alpha,j}(x_0)$ are obtained by solving the ordinary co-kriging system (Wackernagel, 1995).

In our study n_1 and n_j are the same (isotopic case), but that is not the case with heterotopic cokriging or when auxiliary information is exhaustively recorded on a grid (in proximal and remote sensing) (Castrignanò et al., 2009).

It is of paramount importance underlining that the Eq. (3) does not give the expected (mean) value of the indicator but the estimated conditional probability of infection occurrence by using all both binary and numerical available information (Journel, 2011). The Eq. (3) can be extended to any type of auxiliary information including subsoil and nominal variables after transforming the latter to indicator/dummy variables (Goovaerts, 1997).

3. Results

3.1. Drone data

In Fig. 3 the image of the raw drone data in the red-edge band is shown as an example. This band was chosen because, as widely reported in the literature (Horler et al., 1983; Sims and Gamon, 2002; Thenkabail

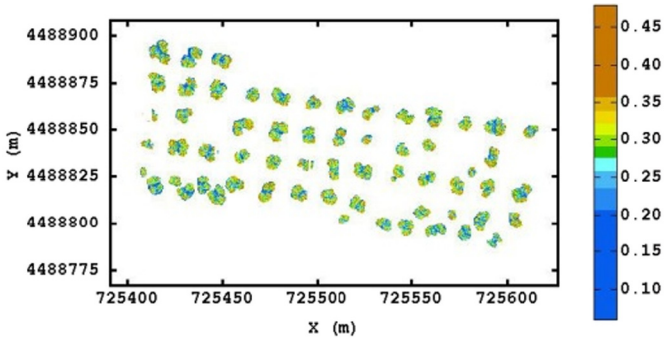

Fig. 3. Drone rededge image of the olive tree canopies.

et al., 2011; Stellacci et al., 2016), its reflectivity is indicative of the healthy conditions of the plant. The onset of any type of stress causes in fact a shift of the rededge towards the red with a lowering of the reflectivity. What is evident from the figure is an extreme variability at a very fine, centimeter scale, so it does not seem obvious to classify the tree according to only one level of severity. This would then cast doubt on the usefulness of assigning a single severity/stress class to the whole plant. However, it was made necessary by the subsequent data fusion analysis since the laboratory analyses were referred to plant scale.

The same type of mathematical model, consisting of an isotropic model with two structures: a nugget effect and a spherical model with range of 5.24 m, was used for all the four bands, whereas the parameters (nugget effect, partial sill) varied for the individual bands. The mathematical type of model was chosen after cross-validation because it was better than others to represent the short-range variation of the canopy. The value of the range was instead estimated by producing a perturbation with 100 simulations until convergence was reached, defined by the threshold value of the mean quadratic error set at 10^{-6}.

The estimated value reflects the average size of the tree, indicating that there is a significant spatial correlation only between the pixels of the same plant, while the between-plant correlation is practically zero or not significant. This might be interpreted as indicative of the extreme stochasticity of the process related to the transmission of infection from a tree to another.

Fig. 4a shows the expected reflectivity values of the 4 bands convoluted at plant level. Although the images are characterized by great between-plant variability, it is possible to notice that the reflectivity values are consistently lower for the plants of the southern edge and the north-west corner, which would indicate a lower vegetative luxuriance. In contrast, the highest reflectivity values are generally found in the central part of the field, where the plants showed less evidence of desiccation as verified by visual inspection.

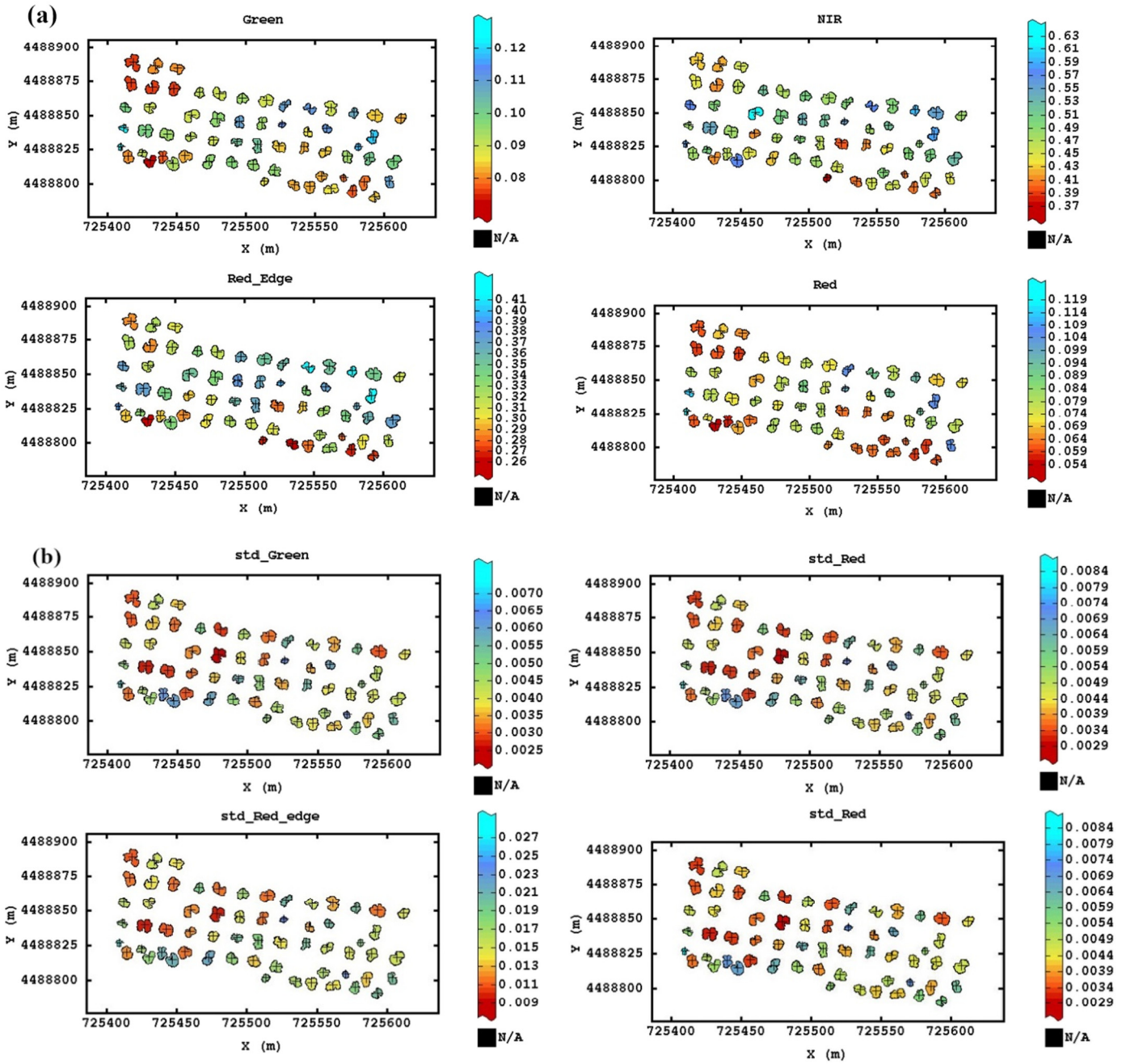

Fig. 4. (a) The expected value of the reflectivity of the four drone bands calculated with polygon kriging at plant level, and (b) the standard deviations of the expected values, respectively.

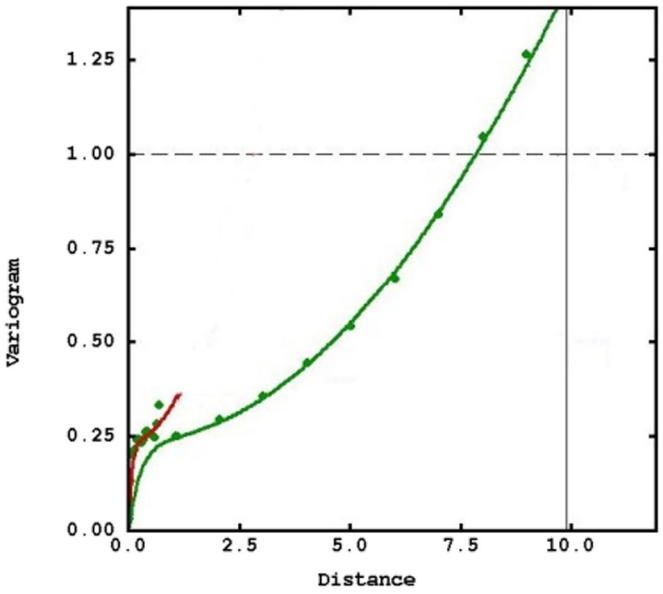

Fig. 5. Example directional variogram (dot) with fitted model (line) of GPR data: spatial (red line) and temporal (green line) variograms. (For interpretation of the references to colour in this figure legend, the reader is referred to the web version of this article.)

Differently, Fig. 4b displays the within-plant variation values (standard deviations) for the single trees related to the reflectivity of the 4 bands. Although also in this case the differences between the single trees are evident, a greater congruence among these maps can be noted than among those of the expected values (Fig. 4a). In fact, it is evident there is a tendency to lower values in the west half of the field than in the east half. This means that the plants in the eastern half present a greater degree of intrinsic tree variability with the various portions of the same canopy having a different degree of vegetative vigour, which may be related to a different local health status though within the same plant.

3.2. GPR data

Since the GPR data showed significant deviations from the normal distribution, to facilitate fitting of the variogram model, they were submitted to a normalizing transformation using a series of Hermite polynomials truncated to the first 100 terms.

The Gaussian transformed data were used to calculate the directional variogram to which an anisotropic model with different ranges in spatial and temporal directions was fitted. As in the case of the drone data, a single mathematical type of anisotropic model was chosen including three main structures: nugget effect, an exponential model and a k- Bessel model. In this case, however, all the parameters of the model: nugget effect, partial sills, parameter of k-Bessel model and ranges were estimated for each tree.

In Fig. 5 the variogram model fitted to the experimental directional variogram is shown as an example. The red curve represents the spatial component, whereas the green one represents the temporal component. The temporal variogram is not upper bounded because it represents a non-stationary process in time, due to the multiple backscattering, which causes the electro-magnetic signal to be extinguished by attenuation.

In Fig. 6 a 2D space-time map of the GPR signal energy is shown as an example. As can be seen, the signal appears reinforced after about 6–7 ns, time probably taken by the signal to reach the opposite end of the trunk. It is for this reason that the Gaussian transformed GPR data were convoluted over this time distance with polygon kriging. We also notice a vertical alternating of zones in the map with different signal energy. Recalling that the intensity of the reflected signal is proportional to the gradient of the dielectric properties of the medium, we can interpret the zones with higher intensity as those characterized by the presence of voids/cavities or with lower water content. The variegated succession of zones with different energy is indicative of the complex trunk morphology of these centenarian olive trees.

In Fig. S2a (supplementary material) the expected values of GPR data convoluted at plant level are shown using symbols of size proportional to value. It is difficult indeed to discover any regularity, since the degree of desiccation of the trunk seems to be randomly distributed. Some particularly dried trunks appear along the edges of the field. The previous considerations for Fig. 8a apply essentially also for Fig. S2b (supplementary material) of the standard deviations, but with a certain prevalence of trees with internally irregular trunks (large standard deviation) along the southern and north-western edges.

Indeed, there is a certain degree of consistency between the drone images (Fig. 4a) and the geophysical images (Fig. S2a), which encourages the use of data fusion techniques of heterogeneous apparently incompatible data, to extract useful indications in the fight against infection.

The same type of graphical representation was used to show the results of the visual investigations of the proportion of dried foliage in the 4 sides of the tree. They reveal that only 5 plants appear more wilted in

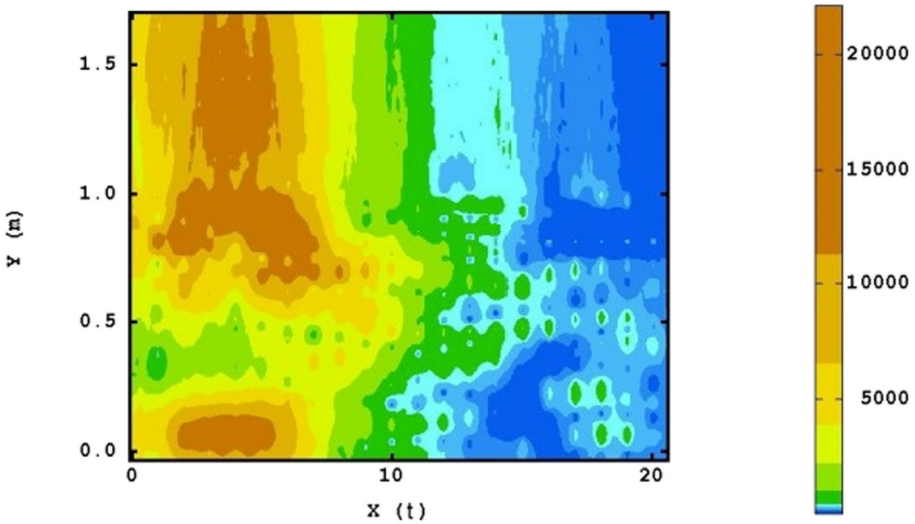

Fig. 6. Example spatial-temporal map of GPR signal.

the northern direction (in the S—W corner, in the middle and in the eastern edge) (Fig. S3a, supplementary material). This result is confirmed also for the east quadrant, even if in this case more plants show intermediate wilting values (Fig. S3b supplementary material). The map for the south quadrant is very similar to that of the north quadrant (Fig. S3c supplementary material) and the map for the west quadrant (Fig. S3d supplementary material) confirms the high degree of desiccation observed for some plants at the eastern edge of the field. However, a difference can be seen in the west map compared to the others: the presence of a plant at the north-west corner that does not appear equally desiccated in the other directions N, E and S.

3.3. Laboratory binary data

The binary (healthy - infected) results of the laboratory analyses (Fig. 7) confirm the presence of the bacterium for the plants with a high degree of desiccation at the NW and SW corners and eastern side. However, in contrast to the previous maps, in which the degree of foliage desiccation appears essentially randomly distributed, laboratory measurements show a clear grouping of infected plants in the eastern part of the field. This suggests that the entry of the insect vectoring *Xfp* occurred from this part of the field, and probably also from the NW and SW corners.

3.4. Multi-source data fusion: probability map of infection risk

An isotropic linear model of co-regionalisation (LMC) was fitted to the set of direct and cross- variograms of the selected 11 variables, consisting of three spatial structures: a nugget effect, a spherical model with range of 40 m; a k-Bessel model with range of 60 m and parameter equal to 1.5. Each spatial component (nugget effect, short range, and long-range structures) explains a percentage of the total variance of 25%, 32%, 43%, respectively. The spatial model then appears well structured with a prevalence of the auto-correlated components (at short and long range) over the uncorrelated error (nugget effect). However, from the graph of the theoretical variograms fitted to the experimental ones (Fig. S4 supplementary material) we notice great dispersion of the experimental points, and low spatial correlation between the indicator and all the auxiliary variables (cross-variograms in the first column on the left of the variogram matrix of Fig. S4 supplementary material). The strength of the spatial correlation is evaluated by the distance between the model and the dashed line (Fig. S4 supplementary material), which represents the condition of intrinsic correlation or maximum correlation (Wackernagel, 1995).

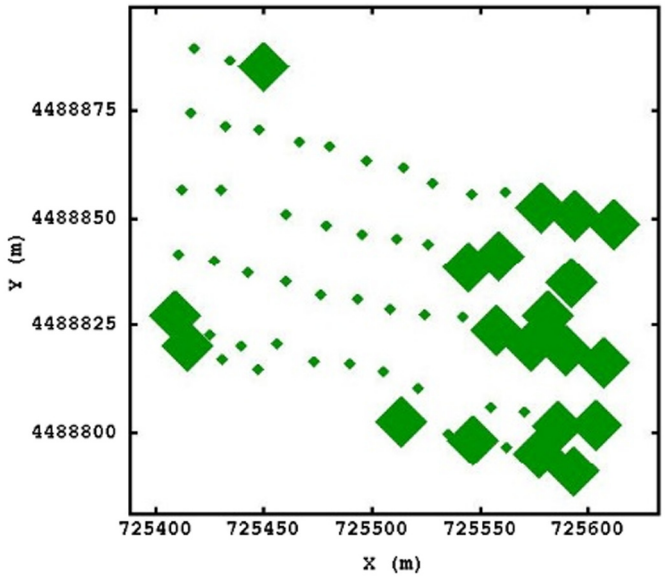

Fig. 7. Base map of binary laboratory data of Xylella infection.

From the visual inspection of the cross-variograms in Fig. S4 (supplementary material) it is also possible to deduce interesting spatial relations between the auxiliary variables: a general positive correlation exists in the visual variables between them, and in the radiometric ones between them, in particular NIR with rededge and green with rededge and red. Differently, geophysical variables do not appear correlated with any of the other variables, probably because of their extreme randomness. Finally, we notice the different shape of the indicator's variogram compared to that of the other variables: being not upper bounded is indicative of a non-steady but evolving process, as one might unfortunately expect.

The spatial dependence model (LMC) was verified through a cross-validation test resulting for the prediction of the indicator variable in the mean and standard deviation of the standardised error by cokriging standard deviation of −0.0064 and 1.1, quite close to 0 and 1, respectively. In addition, the correlation between the residuals and the estimates is 0.083. The model is then unbiased, without systematic errors and sufficiently accurate.

Fig. 8a shows the probability map of the disease occurrence. It is evident how the bacterium through the vector insect has entered from the eastern field edge, and is probably spreading in the *E*-W direction. However, there are two other outbreaks at the NW and SW corners from which the bacterium might also spread.

To follow the progression of the disease leaf samples were taken 6 months later in March 2018 and analysed in the laboratory by quantitative real-time Polymerase Chain Reaction.

The amount of *Xfp* DNA was represented with proportional symbols, and superimposed on the probability map in Fig. 8b. As can clearly be seen after only 6 months, practically all plants were infected, even those located in the central area of the field with an estimated very low probability of infection at the time of the early survey.

These results highlight the extreme rapidity and stochasticity of the spread of the disease and the need for prompt and preventive action with containment measures mainly on infected but asymptomatic plants.

4. Discussion

The previous results of multi-source data processing have showed that the visual evidence confirmed, albeit with a much greater degree of approximation, what was observed with the drone data: the withering process spread essentially randomly even within the same plant, making it really difficult to discover preferential lines of diffusion of the disease. Drone monitoring has revealed that olive trees (both infected and not) are characterized by great variability, coexisting on the same tree parts of the foliage with different vigour.

Moreover, as it results from directional variograms of radiometric data (not shown), spatial variation was essentially isotropic without evident anisotropies along preferential directions of disease propagation even within the same plant.

Although also other researchers (Hornero et al., 2020) have observed the extreme spatio-temporal variability of the infection spreading, influenced by numerous endogenous and exogenous factors to the plant, this type of study is still in its infancy and needs further investigation.

To make even more complex the interpretation of the experimental data, in discovering significant relationships between the occurrence of the disease and various external factors, is also the lack of strong spatial correlation between the infection indicator and the selected auxiliary variables, as evidenced by cross-variograms (Fig. S4 supplementary material). Indeed this lack of spatial correlation might be interpreted also as a scale effect, which means the effect due to the change of support that occurs when variables with different spatial resolution are combined. It is well known that statistical relationships between geo-

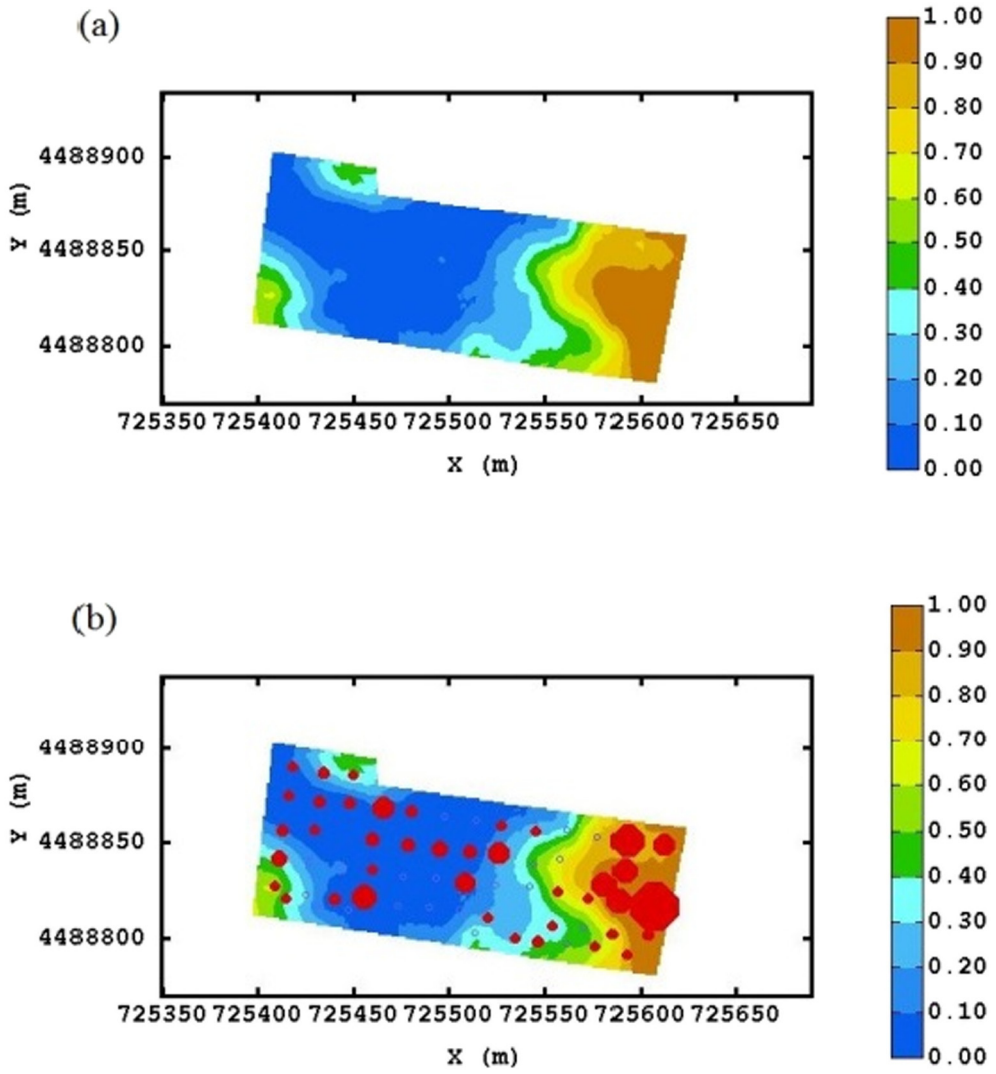

Fig. 8. (a) Probability map of *Xylella fastidiosa* subsp. *pauca* infection. (b) Base map of qPCR measurements in March 2018 superimposed on the probability map.

referenced variables are spatially dependent (King, 2013), i.e. they are affected by spatial scale of survey. Therefore, since the infection by *Xfp* is an essentially punctual event, it would be necessary that all the measurements were carried out at a very fine scale. The scale of the whole plant of laboratory measurements would then seem too coarse and should possibly be reduced, even at leaf scale, in order to identify probable relationships with the much more densely recorded radiometric variables. We believe that these relationships between the radiometric data and the occurrence and severity of the infection exist as was tested by previous experimental evidences indicating that the presence of the bacterium actually causes some alterations in the radiometric response of the olive leaf at well-defined wavelengths (Zarco-Tejada et al., 2018; Hornero et al., 2020; Poblete et al., 2020).

We realize that reducing the scale of laboratory measurement entails the resolution of considerable practical problems, including financial ones, since such measurements are still quite expensive.

However, it is highly to be hoped that research in sensing and statistics will develop to such an extent that the presence of the bacterium can be detected early, even in plants that do not show any symptoms of the disease. To this regard, the results of research applied to hyperspectral sensors is very promising (Poblete et al., 2020).

In light of all above considerations we can conclude that at present it is not easy to predict the spatial and the temporal evolution of the diffusion of *Xfp* infection. There is currently a lack of quantitative assessment of important epidemiological parameters useful for risk analysis and infection management, such as transmission rates, duration of the asymptomatic period or until the plant has dried out and died completely (White et al., 2020).

5. Conclusions

The site-specific management of *Xfp* infections involves the use of different monitoring tools, which can be a powerful aid in containing the bacterium. With the production of big data from modern technology, proximal or remote sensor outputs can be used as auxiliary variables, to supplement information on infection from the primary variable. The latter, resulting from measurements carried out in the laboratory with serological or molecular techniques on plant samples, is for obvious reasons limited. It is therefore necessary to define an effective "data fusion" approach (Dusadeerungsikul et al., 2020; Castrignanò and Buttafuoco, 2020) that combines different types of data in a statistically sound way, in order to obtain a robust estimate. The main objective of this work was to define a "data fusion" procedure, which effectively combines the geo-referenced outputs of various (geophysical and radiometric remote) sensors with point measurements on the ground, for the production of probabilistic maps of infection risk. The approach relies mostly on non-parametric multivariate geostatistics.

The joint analysis of multi-source data poses the crucial problem, unfortunately not yet fully investigated in the scientific literature, of change of support. The future challenge of research will be to define new experimental protocols in which greater spatial congruence between the laboratory measurements and the ones provided by modern proximal and remote monitoring sensors is achieved.

Supplementary data to this article can be found online at https://doi.org/10.1016/j.scitotenv.2020.141814.

CRediT authorship contribution statement

Conceptualization: Castrignanò A., Nigro F., Belmonte A., Quarto R.
Methodology: Castrignano, Belmonte A., Quarto R., Nigro F.
Visualization: Belmonte A., Shaddad S.
Data Curation: Sgrelli S., Confalonieri L, Quarto F, Gadaleta G., Nigro F., Muolo M. R., Ranieri N., Ruggeri S., Shaddad S., Antelmi I., Sion V.
Writing: Original Draft: Castrignanò A., Belmonte A., Riefolo C., Quarto F.
Data Processing: Castrignanò A., Belmonte A., Quarto R., Quarto F.
Supervision: Nigro F.
Writing - Review & Editing: Castrignanò A., Belmonte A., Quarto R., F. Nigro.

Aknowledgements

Project "XylMap - Identification of CoDiRO diffusion dynamics after analysis of progression mechanisms and development of enhanced monitoring and mapping tools and methods" was financed by the Apulia Region (Italy) with reference to DD n. 494 of 14/10/2015 and n. 278 of 9/8/2016 (Cod. A).

Declaration of competing interest

The authors declare that they have no known competing financial interests or personal relationships that could have appeared to influence the work reported in this paper.

References

Allred, B., Eash, N., Freeland, R., Martinez, L., Wishart, D.B., 2018. Effective and efficient agricultural drainage pipe mapping with UAS thermal infrared imagery: a case study. Agric. Water Manag. https://doi.org/10.1016/j.agwat.2017.11.011.

Anderson, M.C., Allen, R.G., Morse, A., Kustas, W.P., 2012. Use of Landsat thermal imagery in monitoring evapotranspiration and managing water resources. Remote Sens. Environ. https://doi.org/10.1016/j.rse.2011.08.025.

Andrio, A., 2019. Development of UAV technology in seed dropping for aerial revegetation practices in Indonesia. IOP Conference Series: Earth and Environmental Science https://doi.org/10.1088/1755-1315/308/1/012051.

Barone, P.M., Ferrara, C., 2019. A posteriori GPR evaluation of tree stability: a case study in Rome (Italy). Remote Sens. https://doi.org/10.3390/rs11111301.

Barton, C.V.M., 2012. Advances in remote sensing of plant stress. Plant Soil https://doi.org/10.1007/s11104-011-1051-0.

Berdugo, C.A., Zito, R., Paulus, S., Mahlein, A.K., 2014. Fusion of sensor data for the detection and differentiation of plant diseases in cucumber. Plant Pathol. https://doi.org/10.1111/ppa.12219.

Bosso, L., Di Febbraro, M., Cristinzio, G., Zoina, A., Russo, D., 2016. Shedding light on the effects of climate change on the potential distribution of Xylella fastidiosa in the Mediterranean basin. Biol. Invasions https://doi.org/10.1007/s10530-016-1118-1.

Buters, Belton, Cross, 2019. Seed and seedling detection using unmanned aerial vehicles and automated image classification in the monitoring of ecological recovery. Drones https://doi.org/10.3390/drones3030053.

Calderón, R., Navas-Cortés, J.A., Lucena, C., Zarco-Tejada, P.J., 2013. High-resolution airborne hyperspectral and thermal imagery for early detection of Verticillium wilt of olive using fluorescence, temperature and narrow-band spectral indices. Remote Sens. Environ. https://doi.org/10.1016/j.rse.2013.07.031.

Campbell, J.B., Wynne, R.H., 2011. Introduction to remote sensing. Uma ética para quantos?, FIFTH edition https://doi.org/10.1007/s13398-014-0173-7.2.

Castrignanò, A., Buttafuoco, G., 2020. In: Castrignanò, A., Buttafuoco, G., Khosla, R., Mouazen, A.M., Moshou, D., Naud, O. (Eds.), Data Processing. Chapter 3 in. Agricultural Internet of Things and Decision Support for Precision Smart Farming, pp. 140–183 AP.

Castrignanò, A., Buttafuoco, G., Canu, A., Zucca, C., Madrau, S., 2008. Modelling spatial uncertainty of soil erodibility factor using joint stochastic simulation. L. Degrad. Dev. https://doi.org/10.1002/ldr.836.

Castrignanò, A., Costantini, E.A.C., Barbetti, R., Sollitto, D., 2009. Accounting for extensive topographic and pedologic secondary information to improve soil mapping. Catena https://doi.org/10.1016/j.catena.2008.12.004.

Castrignanò, A., Buttafuoco, G., Quarto, R., Vitti, C., Langella, G., Terribile, F., Venezia, A., 2017. A combined approach of sensor data fusion and multivariate geostatistics for delineation of homogeneous zones in an agricultural field. Sensors (Switzerland) https://doi.org/10.3390/s17122794.

Chakraborty, A., Seshasai, M.V.R., Dadhwal, V.K., 2016. Assessing crop water stress during late kharif season using normalized diurnal difference vegetation water content (nddVWC) of advanced microwave scanning radiometer–earth observing system (AMSR-E). Nat. Hazards https://doi.org/10.1007/s11069-016-2438-2.

Dai, B., He, Y., Gu, F., Yang, L., Han, J., Xu, W., 2018. A Vision-Based Autonomous Aerial Spray System for Precision Agriculture, in: 2017 IEEE International Conference on Robotics and Biomimetics, ROBIO 2017. https://doi.org/10.1109/ROBIO.2017.8324467.

Diacono, M., Castrignanò, A., Vitti, C., Stellacci, A.M., Marino, L., Cocozza, C., De Benedetto, D., Troccoli, A., Rubino, P., Ventrella, D., 2014. An approach for assessing the effects of site-specific fertilization on crop growth and yield of durum wheat in organic agriculture. Precis. Agric. https://doi.org/10.1007/s11119-014-9347-8.

Diggle, P.J., Serra, J., 1983. Image analysis and mathematical morphology. Biometrics https://doi.org/10.2307/2531038.

Dusadeerungsikul, P.O., Liakos, V., Morari, F., Nof, S.Y., Bechar, A., 2020. Smart action. Agricultural Internet of Things and Decision Support for Precision Smart Farming https://doi.org/10.1016/b978-0-12-818373-1.00005-6.

Faical, B.S., Pessin, G., Filho, G.P.R., Carvalho, A.C.P.L.F., Furquim, G., Ueyama, J., 2014. Fine-tuning of UAV control rules for spraying pesticides on crop fields. Proceedings - International Conference on Tools with Artificial Intelligence, ICTAI https://doi.org/10.1109/ICTAI.2014.85.

Francis, M., Lin, H., Rosa, J.C. La, Doddapaneni, H., Civerolo, E.L., 2006. Genome-based PCR primers for specific and sensitive detection and quantification of Xylella fastidiosa. Eur. J. Plant Pathol. https://doi.org/10.1007/s10658-006-9009-4.

Fu, L., Liu, S., Liu, L., 2014. Internal structure characterization of living tree trunk cross-section using GPR: Numerical examples and field data analysis. Proceedings of the 15th International Conference on Ground Penetrating Radar, GPR 2014 https://doi.org/10.1109/ICGPR.2014.6970405.

Ghulam, A., Li, Z.L., Qin, Q., Yimit, H., Wang, J., 2008. Estimating crop water stress with ETM+ NIR and SWIR data. Agric. For. Meteorol. https://doi.org/10.1016/j.agrformet.2008.05.020.

Gold, K.M., Townsend, P.A., Chlus, A., Herrmann, I., Couture, J.J., Larson, E.R., Gevens, A.J., 2020. Hyperspectral measurements enable pre-symptomatic detection and differentiation of contrasting physiological effects of late blight and early blight in potato. Remote Sens. https://doi.org/10.3390/rs12020286.

Goovaerts, P., 1997. Geostatistics for natural reources evaluation. Geostatistics for natural resources evaluation https://doi.org/10.2307/1270969.

Guthrie, D., Olea, R.A., 1991. Geostatistical glossary and multilingual dictionary. J. Am. Stat. Assoc. https://doi.org/10.2307/2290551.

Han, C., Zhang, H., Gao, C., Jiang, C., Sang, N., Zhang, L., 2016. A remote sensing image fusion method based on the analysis sparse model. IEEE J. Sel. Top. Appl. Earth Obs. Remote Sens. https://doi.org/10.1109/JSTARS.2015.2507859.

Harper, S.J., Ward, L.I., Clover, G.R.G., 2010. Development of LAMP and real-time PCR methods for the rapid detection of Xylella fastidiosa for quarantine and field applications. Phytopathology https://doi.org/10.1094/PHYTO-06-10-0168.

Horler, D.N.H., Dockray, M., Barber, J., 1983. The red edge of plant leaf reflectance. Int. J. Remote Sens. https://doi.org/10.1080/01431168308948546.

Hornero, A., Hernández-Clemente, R., North, P.R.J., Beck, P.S.A., Boscia, D., Navas-Cortes, J.A., et al., 2020. Monitoring the incidence of Xylella fastidiosa infection in olive orchards using ground-based evaluations, airborne imaging spectroscopy and Sentinel-2 time series through 3-D radiative transfer modelling. Remote Sens. Environ. 236, 111480.

Jackson, E.L., Crawford, D.W., Godbey, G., 1993. Negotiation of leisure constraints. Leis. Sci. 15 (1), 1–11.

Journel, A.G., 2011. Fundamentals of Geostatistics in Five Lessons, Fundamentals of Geostatistics in Five Lessons. https://doi.org/10.1029/sc008.

Kerkech, M., Hafiane, A., Canals, R., 2018. Deep leaning approach with colorimetric spaces and vegetation indices for vine diseases detection in UAV images. Comput. Electron. Agric. https://doi.org/10.1016/j.compag.2018.10.006.

King, G., 2013. A solution to the ecological inference problem: Reconstructing individual behavior from aggregate data. A Solution to the Ecological Inference Problem: Reconstructing Individual Behavior from Aggregate Data https://doi.org/10.2307/3341483.

Kogan, F.N., 1995. Droughts of the late 1980s in the United States as derived from NOAA polar-orbiting satellite data. Bull. - Am. Meteorol. Soc. https://doi.org/10.1175/1520-0477(1995)076<0655:DOTLIT>2.0.CO;2.

Landrum, C., Castrignanó, A., Zourarakis, D., Mueller, T., 2016. Assessing the time stability of soil moisture patterns using statistical and geostatistical approaches. Agric. Water Manag. https://doi.org/10.1016/j.agwat.2016.07.013.

Lantuéjoul, C., Serra, J., 1982. M-Filters. ICASSP, IEEE International Conference on Acoustics, Speech and Signal Processing - Proceedings https://doi.org/10.1109/ICASSP.1982.1171856.

Li, W., Wen, J., Xiao, Z., Xu, S., 2018. Application of ground-penetrating radar for detecting internal anomalies in tree trunks with irregular contours. Sensors (Switzerland) https://doi.org/10.3390/s18020649.

Loconsole, G., Potere, O., Boscia, D., Altamura, G., Djelouah, K., Elbeaino, T., Frasheri, D., Lorusso, D., Palmisano, F., Pollastro, P., Silletti, M.R., Trisciuzzi, N., Valentini, F.,

Savino, V., Saponari, M., 2014. Detection of Xylella fastidiosa in olive trees by molecular and serological methods. J. Plant Pathol. https://doi.org/10.4454/JPP.V96I1.041.
Mahlein, A.K., Oerke, E.C., Steiner, U., Dehne, H.W., 2012. Recent advances in sensing plant diseases for precision crop protection. Eur. J. Plant Pathol. https://doi.org/10.1007/s10658-011-9878-z.
Maimaitijiang, M., Sagan, V., Sidike, P., Daloye, A.M., Erkbol, H., Fritschi, F.B., 2020. Crop monitoring using satellite/UAV data fusion and machine learning. Remote Sens. https://doi.org/10.3390/rs12091357.
Maragos, P., 2009. Morphological filtering. The Essential Guide to Image Processing https://doi.org/10.1016/B978-0-12-374457-9.00013-5.
Matheron, G., 1963. Principles of geostatistics. Econ. Geol. https://doi.org/10.2113/gsecongeo.58.8.1246.
Nex, F., Remondino, F., 2014. UAV for 3D mapping applications: a review. Appl. Geomatics. https://doi.org/10.1007/s12518-013-0120-x.
Nixon, M.S., Aguado, A.S., 2012. Basic image processing operations. Feature Extraction & Image Processing for Computer Vision https://doi.org/10.1016/b978-0-12-396549-3.00003-3.
Paredes, J.A., Gonzalez, J., Saito, C., Flores, A., 2017. Multispectral imaging system with UAV integration capabilities for crop analysis. IEEE 1st International Symposium on Geoscience and Remote Sensing, GRSS-CHILE 2017 https://doi.org/10.1109/GRSS-CHILE.2017.7996009.
Parzen, E., 1962. On estimation of a probability density function and mode. Ann. Math. Stat. https://doi.org/10.1214/aoms/1177704472.
Percival, D.B., Walden, A.T., 1993. Spectral Analysis for Physical Applications, Spectral Analysis for Physical Applications. https://doi.org/10.1017/cbo9780511622762.
Poblete, T., Camino, C., Beck, P.S.A., Hornero, A., Kattenborn, T., Saponari, M., Boscia, D., Navas-Cortes, J.A., Zarco-Tejada, P.J., 2020. Detection of Xylella fastidiosa infection symptoms with airborne multispectral and thermal imagery: Assessing bandset reduction performance from hyperspectral analysis. ISPRS J. Photogramm. Remote Sens. https://doi.org/10.1016/j.isprsjprs.2020.02.010.
Rodrigues, J.L.M., Silva-Stenico, M.E., Gomes, J.E., Lopes, J.R.S., Tsai, S.M., 2003. Detection and diversity assessment of Xylella fastidiosa in field-collected plant and insect samples by using 16S rRNA and gyrB sequences. Appl. Environ. Microbiol. https://doi.org/10.1128/AEM.69.7.4249-4255.2003.
Sagan, V., Maimaitijiang, M., Sidike, P., Eblimit, K., Peterson, K.T., Hartling, S., Esposito, F., Khanal, K., Newcomb, M., Pauli, D., Ward, R., Fritschi, F., Shakoor, N., Mockler, T., 2019. UAV-based high resolution thermal imaging for vegetation monitoring, and plant phenotyping using ICI 8640 P, FLIR Vue pro R 640, and thermomap cameras. Remote Sens. https://doi.org/10.3390/rs11030330.
Sankaran, S., Mishra, A., Ehsani, R., Davis, C., 2010. A review of advanced techniques for detecting plant diseases. Comput. Electron. Agric. https://doi.org/10.1016/j.compag.2010.02.007.
Santesteban, L.G., Di Gennaro, S.F., Herrero-Langreo, A., Miranda, C., Royo, J.B., Matese, A., 2017. High-resolution UAV-based thermal imaging to estimate the instantaneous and seasonal variability of plant water status within a vineyard. Agric. Water Manag. https://doi.org/10.1016/j.agwat.2016.08.026.
Saponari, M., Boscia, D., Nigro, F., Martelli, G.P., 2013. Identification of dna sequences related to Xylella fastidiosa in oleander, almond and olive trees exhibiting leaf scorch symptoms in Apulia (Southern Italy). J. Plant Pathol. https://doi.org/10.4454/JPP.V95I3.035.
Saponari, M., Boscia, D., Altamura, G., Loconsole, G., Zicca, S., D'Attoma, G., Morelli, M., Palmisano, F., Saponari, A., Tavano, D., Savino, V.N., Dongiovanni, C., Martelli, G.P., 2017. Isolation and pathogenicity of Xylella fastidiosa associated to the olive quick decline syndrome in southern Italy. Sci. Rep. https://doi.org/10.1038/s41598-017-17957-z.
Saponari, M., Giampetruzzi, A., Loconsole, G., Boscia, D., Saldarelli, P., 2019. Xylella fastidiosa in olive in Apulia: where we stand. Phytopathology 109, 175–186.
Schneider, K., van der Werf, W., Cendoya, M., Mourits, M., Navas-Cortés, J.A., Vicent, A., Lansink, A.O., 2020. Impact of Xylella fastidiosa subspecies pauca in European olives. Proc. Natl. Acad. Sci. U. S. A. https://doi.org/10.1073/pnas.1912206117.
Seguin, B., Lagouarde, J.P., Savane, M., 1991. The assessment of regional crop water conditions from meteorological satellite thermal infrared data. Remote Sens. Environ. https://doi.org/10.1016/0034-4257(91)90007-S.
Shaddad, S.M., Buttafuoco, G., Castrignanò, A., 2020. Assessment and mapping of soil salinization risk in an Egyptian field using a probabilistic approach. Agronomy https://doi.org/10.3390/agronomy10010085.
Sheriff, R.E., 2002. Encyclopedic Dictionary of Applied Geophysics, Encyclopedic Dictionary of Applied Geophysics. https://doi.org/10.1190/1.9781560802969.
Sims, D.A., Gamon, J.A., 2002. Relationships between leaf pigment content and spectral reflectance across a wide range of species, leaf structures and developmental stages. Remote Sens. Environ. https://doi.org/10.1016/S0034-4257(02)00010-X.
Steele-Dunne, S.C., McNairn, H., Monsivais-Huertero, A., Judge, J., Liu, P.W., Papathanassiou, K., 2017. Radar remote sensing of agricultural canopies: a review. IEEE J. Sel. Top. Appl. Earth Obs. Remote Sens. https://doi.org/10.1109/JSTARS.2016.2639043.
Stellacci, A.M., Castrignanò, A., Troccoli, A., Basso, B., Buttafuoco, G., 2016. Selecting optimal hyperspectral bands to discriminate nitrogen status in durum wheat: a comparison of statistical approaches. Environ. Monit. Assess. https://doi.org/10.1007/s10661-016-5171-0.
Sternberg, S.R., 1983. Biomedical image processing. Computer (Long. Beach. Calif) https://doi.org/10.1109/MC.1983.1654163.
Thenkabail, A., Lyon, P., Huete, J., Thenkabail, P., Lyon, J., Huete, A., 2011. Advances in Hyperspectral remote sensing of vegetation and agricultural croplands. Hyperspectral Remote Sensing of Vegetation https://doi.org/10.1201/b11222-3.
Wackernagel, H., 1995. Multivariate geostatistics: an introduction with applications. Multivar. Geostatistics an Introd. With Appl. https://doi.org/10.2307/2291758.
Wen, J., Gao, L., Xiao, X., Xiao, Z., Li, C., 2016. Detection and measurement of internal defects for tree trunk by GPR. Int. J. Simul. Syst. Sci. Technol. https://doi.org/10.5013/IJSSST.a.17.31.09.
West, J.S., Bravo, C., Oberti, R., Lemaire, D., Moshou, D., McCartney, H.A., 2003. The potential of optical canopy measurement for targeted control of field crop diseases. Annu. Rev. Phytopathol. 41, 593–614.
White, S., Navas-Cortés, J., Bullock, J., Boscia, D., Chapman, D., 2020. Estimating the epidemiology of emerging *Xylella fastidiosa* outbreaks in olives. Plant Pathol. https://doi.org/10.1111/ppa.13238 Accepted Author Manuscript.
Zarco-Tejada, P.J., Camino, C., Beck, P.S.A., Calderon, R., Hornero, A., Hernández-Clemente, R., Kattenborn, T., Montes-Borrego, M., Susca, L., Morelli, M., Gonzalez-Dugo, V., North, P.R.J., Landa, B.B., Boscia, D., Saponari, M., Navas-Cortes, J.A., 2018. Previsual symptoms of Xylella fastidiosa infection revealed in spectral plant-trait alterations. Nat. Plants. https://doi.org/10.1038/s41477-018-0189-7.
Zhang, J., Huang, Y., Pu, R., Gonzalez-Moreno, P., Yuan, L., Wu, K., Huang, W., 2019. Monitoring plant diseases and pests through remote sensing technology: a review. Comput. Electron. Agric. https://doi.org/10.1016/j.compag.2019.104943.
Zheng, H., Zhou, X., Cheng, T., Yao, X., Tian, Y., Cao, W., Zhu, Y., 2016. Evaluation of a UAV-based hyperspectral frame camera for monitoring the leaf nitrogen concentration in rice. International Geoscience and Remote Sensing Symposium (IGARSS) https://doi.org/10.1109/IGARSS.2016.7730917.
Zovko, M., Romić, D., Colombo, C., Di Iorio, E., Romić, M., Buttafuoco, G., Castrignanò, A., 2018. A geostatistical Vis-NIR spectroscopy index to assess the incipient soil salinization in the Neretva River valley, Croatia. Geoderma. https://doi.org/10.1016/j.geoderma.2018.07.005.